Biomedical Optics EXPRESS

Non-contact acoustic radiation force impulse microscopy via photoacoustic detection for probing breast cancer cell mechanics

Jae Youn Hwang,[1] Bong Jin Kang,[2] Changyang Lee,[2] Hyung Ham Kim,[2] Jinhyoung Park,[2,4,*] Qifa Zhou,[2,3,4] and K. Kirk Shung[2]

[1]*Department of Information and Communication Engineering, Daegu Gyeongbuk Institute of Science & Technology, Daegu, South Korea*
[2]*Department of Biomedical Engineering, University of Southern California, Los Angeles, CA 90089, USA*
[3]*Co-corresponding authors*
[4]*qifazhou@usc.edu*
[*]*jinhyoung.park@gmail.com*

Abstract: We demonstrate a novel non-contact method: acoustic radiation force impulse microscopy via photoacoustic detection (PA-ARFI), capable of probing cell mechanics. A 30 MHz lithium niobate ultrasound transducer is utilized for both detection of phatoacoustic signals and generation of acoustic radiation force. To track cell membrane displacements by acoustic radiation force, functionalized single-walled carbon nanotubes are attached to cell membrane. Using the developed microscopy evaluated with agar phantoms, the mechanics of highly- and weakly-metastatic breast cancer cells are quantified. These results clearly show that the PA-ARFI microscopy may serve as a novel tool to probe mechanics of single breast cancer cells.

©2014 Optical Society of America

OCIS codes: (170.7170) Ultrasound; (170.5120) Photoacoustic imaging; (170.0180) Microscopy.

References and links

1. Y. L. Wang and D. E. Discher, *Cell Mechanics* (Academic Press, San Diego, 2007).
2. H. W. Hou, A. A. Bhagat, A. G. Chong, P. Mao, K. S. Tan, J. Han, and C. T. Lim, "Deformability based cell margination--a simple microfluidic design for malaria-infected erythrocyte separation," Lab Chip **10**(19), 2605–2613 (2010).
3. J. L. Maciaszek and G. Lykotrafitis, "Sickle cell trait human erythrocytes are significantly stiffer than normal," J. Biomech. **44**(4), 657–661 (2011).
4. W. Xu, R. Mezencev, B. Kim, L. Wang, J. McDonald, and T. Sulchek, "Cell stiffness is a biomarker of the metastatic potential of ovarian cancer cells," PLoS ONE **7**(10), e46609 (2012).
5. H. Zhang and K. K. Liu, "Optical tweezers for single cells," J. R. Soc. Interface **5**(24), 671–690 (2008).
6. R. M. Hochmuth, "Micropipette aspiration of living cells," J. Biomech. **33**(1), 15–22 (2000).
7. B. Fabry, G. N. Maksym, R. D. Hubmayr, J. P. Butler, and J. J. Fredberg, "Implications of heterogeneous bead behavior on cell mechanical properties measured with magnetic twisting cytometry," J. Magn. Magn. Mater. **194**(1-3), 120–125 (1999).
8. F. Rico, P. Roca-Cusachs, N. Gavara, R. Farré, M. Rotger, and D. Navajas, "Probing mechanical properties of living cells by atomic force microscopy with blunted pyramidal cantilever tips," Phys. Rev. E Stat. Nonlin. Soft Matter Phys. **72**(2), 021914 (2005).
9. M. Musielak, "Red blood cell-deformability measurement: review of techniques," Clin. Hemorheol. Microcirc. **42**(1), 47–64 (2009).
10. P. Pravincumar, D. L. Bader, and M. M. Knight, "Viscoelastic cell mechanics and actin remodelling are dependent on the rate of applied pressure," PLoS ONE **7**(9), e43938 (2012).
11. D. Kilinc and G. U. Lee, "Advances in magnetic tweezers for single molecule and cell biophysics," Integrative biology: Quantitative Biosciences from Nano to Macro **6**(1), 27–34 (2013).
12. A. R. Bausch, W. Möller, and E. Sackmann, "Measurement of local viscoelasticity and forces in living cells by magnetic tweezers," Biophys. J. **76**(1), 573–579 (1999).

#221587 - $15.00 USD Received 26 Aug 2014; revised 25 Sep 2014; accepted 2 Oct 2014; published 3 Dec 2014

13. D. Dumont, J. Dahl, E. Miller, J. Allen, B. Fahey, and G. Trahey, "Lower-limb vascular imaging with acoustic radiation force elastography: demonstration of in vivo feasibility," IEEE Trans. Ultrason. Ferroelectr. Freq. Control **56**(5), 931–944 (2009).
14. K. Nightingale, M. S. Soo, R. Nightingale, and G. Trahey, "Acoustic radiation force impulse imaging: in vivo demonstration of clinical feasibility," Ultrasound Med. Biol. **28**(2), 227–235 (2002).
15. K. R. Nightingale, P. J. Kornguth, W. F. Walker, B. A. McDermott, and G. E. Trahey, "A novel ultrasonic technique for differentiating cysts from solid lesions: preliminary results in the breast," Ultrasound Med. Biol. **21**(6), 745–751 (1995).
16. M. L. Palmeri, K. D. Frinkley, L. Zhai, M. Gottfried, R. C. Bentley, K. Ludwig, and K. R. Nightingale, "Acoustic radiation force impulse (ARFI) imaging of the gastrointestinal tract," Ultrason. Imaging **27**(2), 75–88 (2005).
17. F. Viola, M. D. Kramer, M. B. Lawrence, J. P. Oberhauser, and W. F. Walker, "Sonorheometry: a noncontact method for the dynamic assessment of thrombosis," Ann. Biomed. Eng. **32**(5), 696–705 (2004).
18. J. Park, J. Lee, S. T. Lau, C. Lee, Y. Huang, C. L. Lien, and K. Kirk Shung, "Acoustic radiation force impulse (ARFI) imaging of zebrafish embryo by high-frequency coded excitation sequence," Ann. Biomed. Eng. **40**(4), 907–915 (2012).
19. J. Y. Hwang, N. S. Lee, C. Lee, K. H. Lam, H. H. Kim, J. Woo, M. Y. Lin, K. Kisler, H. Choi, Q. Zhou, R. H. Chow, and K. K. Shung, "Investigating Contactless High Frequency Ultrasound Microbeam Stimulation for Determination of Invasion Potential of Breast Cancer Cells," Biotechnol. Bioeng. **110**(10), 2697–2705 (2013).
20. T. A. Hall, M. Bilgen, M. F. Insana, and T. A. Krouskop, "Phlantom Materials for Elastography," IEEE Trans. Ultrason. Ferroelectr. Freq. Control **44**(6), 1355–1365 (1997).
21. T. Ramanathan, F. T. Fisher, R. S. Ruoff, and L. C. Brinson, "Amino-Functionalized Carbon Nanotubes for Binding to Polymers and Biological Systems," Chem. Mater. **17**(6), 1290–1295 (2005).
22. J. Park, C. Hu, X. Li, Q. Zhou, and K. K. Shung, "Wideband linear power amplifier for high-frequency ultrasonic coded excitation imaging," IEEE Trans. Ultrason. Ferroelectr. Freq. Control **59**(4), 825–832 (2012).
23. J. Lee, S. Y. Teh, A. Lee, H. H. Kim, C. Lee, and K. K. Shung, "Transverse acoustic trapping using a gaussian focused ultrasound," Ultrasound Med. Biol. **36**(2), 350–355 (2010).
24. B. C. Kuo, Theory and applications of step motors (West Pub. Co., St. Paul, 1974).
25. L. Deng, S. J. Eichhorn, C. C. Kao, and R. J. Young, "The effective Young's modulus of carbon nanotubes in composites," ACS Appl. Mater. Interfaces **3**(2), 433–440 (2011).
26. V. Swaminathan, K. Mythreye, E. T. O'Brien, A. Berchuck, G. C. Blobe, and R. Superfine, "Mechanical stiffness grades metastatic potential in patient tumor cells and in cancer cell lines," Cancer Res. **71**(15), 5075–5080 (2011).
27. J. Guck, S. Schinkinger, B. Lincoln, F. Wottawah, S. Ebert, M. Romeyke, D. Lenz, H. M. Erickson, R. Ananthakrishnan, D. Mitchell, J. Käs, S. Ulvick, and C. Bilby, "Optical deformability as an inherent cell marker for testing malignant transformation and metastatic competence," Biophys. J. **88**(5), 3689–3698 (2005).
28. N. Walter, T. Busch, T. Seufferlein, and J. P. Spatz, "Elastic moduli of living epithelial pancreatic cancer cells and their skeletonized keratin intermediate filament network," Biointerphases **6**(2), 79–85 (2011).
29. S. Suresh, "Nanomedicine: elastic clues in cancer detection," Nat. Nanotechnol. **2**(12), 748–749 (2007).
30. C. K. Leung, C. Ye, and R. N. Weinreb, "An Ultra-High-Speed Scheimpflug Camera for Evaluation of Corneal Deformation Response and Its Impact on IOP Measurement," Invest. Ophthalmol. Vis. Sci. **54**(4), 2885–2892 (2013).
31. L. P. Zanello, B. Zhao, H. Hu, and R. C. Haddon, "Bone cell proliferation on carbon nanotubes," Nano Lett. **6**(3), 562–567 (2006).
32. K. H. Park, M. Chhowalla, Z. Iqbal, and F. Sesti, "Single-walled carbon nanotubes are a new class of ion channel blockers," J. Biol. Chem. **278**(50), 50212–50216 (2003).
33. P. Cherukuri, S. M. Bachilo, S. H. Litovsky, and R. B. Weisman, "Near-infrared fluorescence microscopy of single-walled carbon nanotubes in phagocytic cells," J. Am. Chem. Soc. **126**(48), 15638–15639 (2004).
34. N. W. Shi Kam, T. C. Jessop, P. A. Wender, and H. Dai, "Nanotube molecular transporters: internalization of carbon nanotube-protein conjugates into Mammalian cells," J. Am. Chem. Soc. **126**(22), 6850–6851 (2004).
35. H. Dumortier, S. Lacotte, G. Pastorin, R. Marega, W. Wu, D. Bonifazi, J. P. Briand, M. Prato, S. Muller, and A. Bianco, "Functionalized carbon nanotubes are non-cytotoxic and preserve the functionality of primary immune cells," Nano Lett. **6**(7), 1522–1528 (2006).
36. A. A. Shvedova, V. Castranova, E. R. Kisin, D. Schwegler-Berry, A. R. Murray, V. Z. Gandelsman, A. Maynard, and P. Baron, "Exposure to carbon nanotube material: assessment of nanotube cytotoxicity using human keratinocyte cells," J. Toxicol. Environ. Health A **66**(20), 1909–1926 (2003).
37. M. M. Frigault, J. Lacoste, J. L. Swift, and C. M. Brown, "Live-cell microscopy - tips and tools," J. Cell Sci. **122**(6), 753–767 (2009).
38. C. L. Bayer, J. Kelvekar, and S. Y. Emelianov, "Influence of nanosecond pulsed laser irradiance on the viability of nanoparticle-loaded cells: implications for safety of contrast-enhanced photoacoustic imaging," Nanotechnology **24**(46), 465101 (2013).

#221587 - $15.00 USD Received 26 Aug 2014; revised 25 Sep 2014; accepted 2 Oct 2014; published 3 Dec 2014
(C) 2014 OSA

1. Introduction

Cellular mechanics may play a crucial role in the differentiation, migration, gene expression of cells [1]. Mechanical properties of a cell can be changed by various external and internal cues including disease infection and variations in cell nature. Diseased cells undergo variations in cellular compositions, internal structures, and external interactions, which are closely related to the changes in mechanical properties of cells. For example, malaria infected red blood cells initiate erythrocytic stages of their life cycle, thereby resulting in the cells' progressive stiffening [2]. Erythrocytes from patients with sickle cell disease exhibit higher Young's modulus than normal erythrocytes [3]. In addition, the mechanical properties of cells have been shown to differ as their phenotypes. In particular, metastatic cancer cells, which remodel internal structures of actin cytoskeletons, are reported to be less stiff than weakly-metastatic cancer cells [4]. As shown in these previous studies, the cell mechanics can be altered by disease infection, variations in cell phenotype, and etc. Therefore, the measurement of mechanical properties of single cells may provide important clues to the identification of cellular phenotypes, alternations, and functions.

Various techniques including optical tweezers [5], micropipette aspiration [6], magnetic tweezers [7] and atomic force microscopy (AFM) [8] have been developed to measure the mechanical properties of various cells. Using optical tweezers, the shear modulus of a red blood cell was successfully measured by trapping two microspheres attached to the opposite sides of the red blood cell [9]. However, when the trapping forces were applied to the cells via optical tweezers, it was necessary to tightly focus laser beams on microbeads attached to the cells in order to avoid the cell damages induced by temperature rise [9]. AFM allows measurement of the stiffness of cells with a Young's modulus of greater than 50 Pa. However, the AFM indentation method requires a probe to be in contact of a cell. In addition, the AFM system must be isolated from surrounding vibrations to produce the reliable outcomes [8]. Micropipette aspiration, capable of measuring the amount of surface extension caused by the aspirating pressure, is a versatile approach for measuring cellular mechanical properties due to the broad range of its applicable pressure. Recently, this method has been employed to determine the viscosity and actin remodeling of isolated chondrocytes [10]. However, in spite of its broad range of applications, the reliability of outcomes obtained with this technique has been shown to be highly dependent on the operator's skills and also affected by the unstable base pressure due to potential vapor evaporation in the aspiration chamber [6]. Magnetic tweezers have been also utilized to measure mechanical properties of various biological samples including individual molecules, inter-molecular bonds, and whole cells. They are capable of measuring not only the complex modulus of elasticity but also the local viscoelasticity of the cells [11]. However, for successful quantification of viscoelastic properties of target cells, both generation of highly localized magnetic fields and field gradients and spherical magnetic beads with various sizes are required [12].

In addition to the aforementioned methods, ultrasonic techniques may be employed as an alternative to measure cell mechanics. Particularly, the ultrasonic method would be highly useful as a non-contact method for measurement of the mechanics of a single cell. In recent years, the acoustic radiation force impulse (ARFI) imaging techniques have been developed as a non-invasive method for quantitative measurement of elastic properties of tissues [13]. The ARFI imaging utilizes short duration acoustic radiation forces in order to induce localized displacements in tissue. Such displacements in the order of ten microns are then tracked using ultrasonic correlation based methods. The displacements are typically inversely proportional to local tissue stiffness, thus enabling the estimation of tissue visco-elastic properties. In this method, the short duration acoustic radiation forces are exerted in the direction of acoustic wave propagation by a transfer of momentum from the acoustic wave to a target medium. The momentum transfer here results in the application of a mechanical force to the target. The exerted force can be expressed with the following equation:

#221587 - $15.00 USD Received 26 Aug 2014; revised 25 Sep 2014; accepted 2 Oct 2014; published 3 Dec 2014
(C) 2014 OSA

$$F = \frac{W_{absorbed}}{c} = \frac{2\alpha I}{c}. \quad (1)$$

where F [dyn (1000 cm)$^{-3}$], or [kg s^{-2} cm^{-2}] is acoustic radiation force, $W_{absorbed}$ [W (100 cm)$^{-3}$] is the power absorbed by the medium at a given spatial location, c [m s^{-1}] is the speed of sound in the medium, α [m^{-1}] is the absorption coefficient of the medium, and I [W cm^{-2}] is the temporal average intensity at a given point in space [14]. Currently, a few ARFI imaging techniques have been utilized for various biological applications including *in vivo* discrimination of cysts from solid lesions by estimating the visco-elastic properties of the target [15], detection of lesions in the gastrointestinal tract [16], and assessment of the mechanical properties of coagulations with minimal disturbances [17]. More recently, we have shown that mechanical properties of the internal micro-structures of a zebrafish embryo of a size of ~800 µm could be successfully estimated with high frequency ARFI imaging at 100 MHz, yielding a 2D map of mechanical properties of the zebrafish embryo [18]. However, for ARFI imaging of a single cell, which typically have a dimension in the order of tens of micrometers, the operating frequency of a transducer needs to be further increased to beyond 300 MHz, which offers an axial resolution of ~5µm, to resolve a single cell from the cell culture substrate, which typically produces much stronger echo signals than a cell. Meanwhile, the sensitivity of the transducer used for the ARFI imaging needs to be increased since the acoustic characteristics of cells are close to those of water, producing extremely weak echo signals from cells in a cell culture medium. However, the design and fabrication of such transducers currently remains to be a great challenge.

In this paper, we therefore present a novel *non-contact* ARFI microscopic approach based on photoacoustic detection (PA-ARFI) to probe mechanical properties of a single cell at 30 MHz, which is much lower than the frequency required for ultrasonic approaches. Functionalized single-walled carbon nanotubes (FCNT), which produce strong photoacoustic signals, were here utilized as contrast agents for cell membrane labeling to track displacements of cell membrane due to acoustic radiation force acting on the cells. Note that the cell culture substrate does not generate detectable photoacoustic signals, avoiding interference signals generated by the substrate frequently encountered in ultrasonic approaches. For evaluation of the PA-ARFI microscopy, elasticity of agar phantoms of different Young's modulus is examined. We furthermore investigate whether PA-ARFI microscopy is capable of detecting acoustic radiation force-induced membrane displacement of breast cancer cells, including highly invasive (MDA-MB-231) and weakly invasive (SKBR3 and MCF-7) cells [19], thereby demonstrating the potential of PA-ARFI microscopy in probing mechanical properties of single cells.

2. Materials and methods

2.1 Cell preparation and materials

MDA-MB-231, SKBR3, and MCF-7 human breast cancer cell lines were obtained from the ATCC (Manassas, VA), and maintained in Dulbecco's modified eagle medium (DMEM) containing 10% fetal bovine serum. NH2 functionalized single-walled carbon nanotubes (FCNT) were purchased from Cheap Tubes Inc. (Brattleboro, Vermont). Agar powder (SIGMA-ALDRICH, USA) was prepared for construction of phantoms. Hank's balanced salt solution (HBSS) was purchased from Invitrogen (Grand Island, NY) for maintaining cells during cell experiment. Rhodamine B was purchased from SIGMA-ALDRICH (USA).

2.2 Construction of tissue-mimicking phantoms with different elasticity

In order to evaluate the performance of PA-ARFI microscopy, tissue-mimicking phantoms of different Young's modulus were made with agar gel in a 35 mm petri-dish as described previously [20]. The phantom consisted of three layers including a substrate, an agar gel, and

#221587 - $15.00 USD Received 26 Aug 2014; revised 25 Sep 2014; accepted 2 Oct 2014; published 3 Dec 2014
(C) 2014 OSA

a FCNT layer. In the construction of the phantoms, agar powder was hydrated with deionized water containing n-propanol and then slowly stirred to avoid clumps, followed by degassing of the mixture in a vacuum (660–730 mmHg) for a few minutes. The mixture was initially heated at 70°C in water for colloid dispersion and gas release, and its temperature was further increased up to 90°C. The mixture was then quickly vacuumed to remove residual air bubbles and rotated for obtaining homogeneous agar and cooled down to 45 °C for cross-linking, before being poured into the petri-dish to produce an agar phantom. Finally, FCNTs were spread on the surface of the agar layer before the agar gel was firmly solidified. The thickness of the agar gel layer was ~4 mm. After the construction of each phantom with different Young's modulus, the mechanical properties of the constructed agar phantoms were measured with an Electro Force Load Frame System to confirm whether the mechanical properties of the phantoms were produced as designed (BOSE 3100, USA). The software incorporated with the system was utilized to obtain Young's moduli of the phantoms.

2.3 Evaluation of the PA-ARFI microscopic method

For evaluation of the PA-ARFI microscopic system, we investigated the capability in the detection of axial displacement of a target sample. We further examined elastic properties of the constructed phantoms with different Young's moduli, 0.7 and 1.7kPa using the PA-ARFI system. In the investigation of detection capability of the system, FCNTs diluted with HBSS (10μg/ml) were added into petri-dish, followed by washing with HBSS after 4 hours. The targeted FCNTs bound to the surface of the petri-dish were then searched after placing the sample on a micro-stage of the PA-ARFI system and positioned at the center of an image field of view. PA-signals from the targeted FCNTs were then detected by the transducer used in the PA-ARFI system at the indicated z-positions, respectively (0-1.5μm, step size: 0.5μm). In the phantom study, after the targeted FCNTs in each phantom were searched, the FCNTs were positioned at the center of the image field of view using x-, y-stage manipulators incorporated into the system. Displacements of the FCNTs due to acoustic radiation forces were measured at the given driving voltage inputs to the transducer, 2, 10, 20, 30, and 40 V_{pp}, respectively (number of cycles: 5000). The experiment was repeated 5 times.

2.4 Measurement of mechanical properties of breast cancer cells using PA-ARFI microscopy

10^5 MDA-MB-231, SKBR3, MCF-7 human breast cancer cells were plated on 35mm petri-dishes and incubated in the complete medium at 37°C for 36 hours prior to FCNT labeling of the cells. For the FCNT labeling of the cells, FCNTs diluted with HBSS (final concentration: 0.1μg/ml) were added into the petri-dishes, rocked for 30 minutes, and then incubated at 37°C for 4 hours. The amine-terminated end of FCNTs allowed to be attached to biological systems such as DNA and carbohydrates [21]. After 4 hour incubation of the cells, the cells were washed with HBSS three times and then placed on the microscope to estimate elasticity of each type of cells [sample number (n): 30] using the PA-ARFI microscopy as the procedures described next:(a) the acoustic transducer surface was immerged into the HBSS medium; (b) the location along the z-direction is adjusted for locating a target cell at the focal point of the transducer; (c) the target cell labeled with FCNTs was positioned at the center of the image field of view; (d) acoustic radiation force impulses were applied to the target cell; (e) cell membrane displacements were tracked by measurement of PA signals from the FCNTs binding to cell membrane.

2.5 Data analysis

The acquired PA signals were sampled up to 2 GHz with polynomial interpolation filters with symmetric coefficients in order to quantify the displacement of a target due to acoustic radiation forces acting on the target. Cross-correlation calculation between the reference and track PA signals was then performed to obtain the maximum displacement. A threshold of 0.8 was set for the correlation coefficient for data analysis [18].

#221587 - $15.00 USD Received 26 Aug 2014; revised 25 Sep 2014; accepted 2 Oct 2014; published 3 Dec 2014
(C) 2014 OSA

2.6 Statistical analysis

The membrane displacements of MDA-MB-231 (n = 30), SKBR3 (n = 21), and MCF-7 (n = 10) cells due to acoustic radiation forces acting on the cells were compared. All data were expressed as mean ± standard deviation of indicated sample sizes, and were analyzed by a two-tailed t-test, with the level of significance set at *p-value* <0.01.

3. Results and discussion

3.1 PA-ARFI system

A PA-ARFI system was developed with an inverted microscope (Olympus IX71, USA) [Fig. 1(a)]. A pulsed laser light at 532 nm (Explorer, Spectra-physics) with the pulse energy of 18µJ corresponding to the pulse length of 15 ns was delivered to a target of interest by a beam expander (Thorlabs, USA), a set of mirrors, an electronic shutter, dichroic mirrors, a diffuser, and a 20x objective for PA signal generation within the target. Note that the beam expander and diffuser offered full-field and relatively uniform excitation of the target sample. A single element 30MHz lithium niobate ($LiNbO_3$) ultrasound transducer was fabricated and attached to a goniometer coupled to a three-axis linear motorized stage integrated with the microscope to both detect PA signals and generate acoustic radiation force. The PA signals from the target sample were detected by the transducer and then amplified with an analog receiver (Panametrics, Olympus). The amplified signals were digitized by an analog-to-digital converter (Gage, USA) at 2 GHz sampling rate allowing detection at least 0.75 µm displacement of a target and recorded by a custom-built program developed in house. Here, the transducer and laser were synchronized by a trigger impulse, which was generated at 20 kHz from a function generator (Tektronix, USA).

Multi-cycle 30 MHz sinusoidal bursts generated from a function generator (Tektronix, USA) were amplified by a custom-built power amplifier (gain: 26dB) [22] and input to the transducer for the generation of an acoustic pushing beam at a pulse repetition frequency (PRF) of 20 kHz, which was used to trigger the laser controller for synchronization. Figure 1(b) illustrates triggering sequences for the PA-ARFI system. After initiation of PA-ARFI measurement, laser pulses to generate the reference PA signal were applied to a target sample prior to the application of one pushing beam of five thousands cycles to the sample. After the application of the pushing beam to the sample is completed, five hundred photoacoustic signals generated by the consecutive laser pulses applied to the sample were utilized for tracking its displacement. Note that the photoacoustic signals while the pushing beam transmits were ignored.

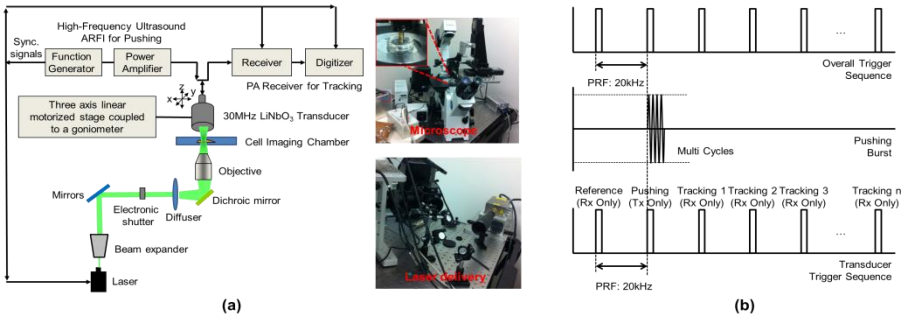

Fig. 1. PA-ARFI system. (a) Schematic of a PA-ARFI system and its photographs. (b) Triggering sequences for the PA-ARFI method.

#221587 - $15.00 USD Received 26 Aug 2014; revised 25 Sep 2014; accepted 2 Oct 2014; published 3 Dec 2014
(C) 2014 OSA

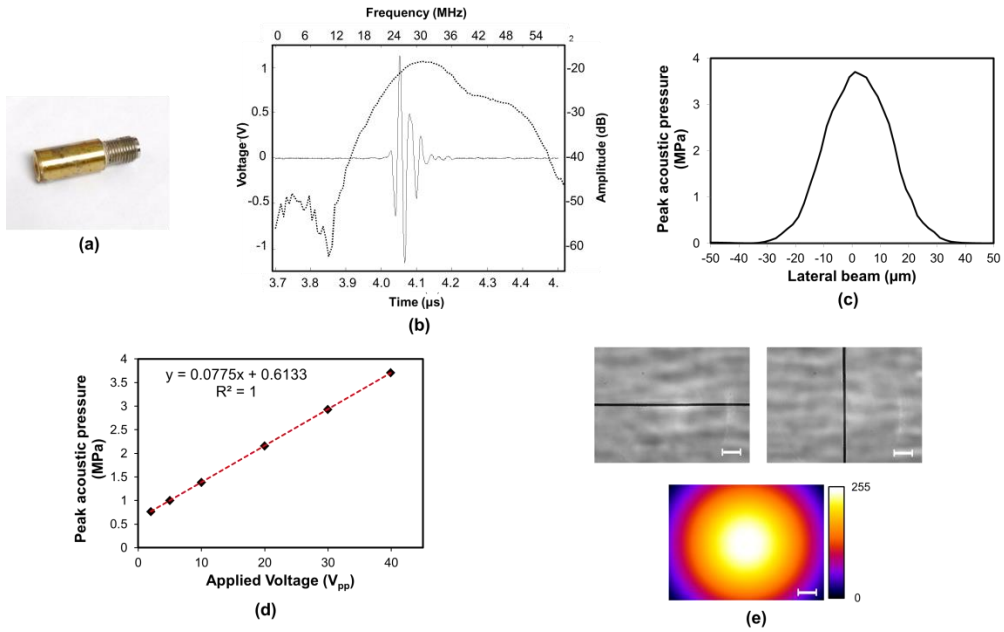

Fig. 2. Characteristics and alignment of the press-focused 30 MHz single element LiNbO3 transducer. (a) Photographic image of the transducer. (b) Pulse-echo characteristics of the transducer. (c) Lateral beam profile of a transducer. (d) Peak acoustic pressures at indicated voltage inputs to the transducer were measured by using a hydrophone. (e) Alignment of a laser beam (below) to the transducer's focus was made by using a 6µm tungsten wire targets aligned along the horizontal (upper-left) and vertical (upper-right) direction at the center of the image and fluorescence imaging of 10 µM Rhodamine B solution. The scale bars indicate 50 µm.

In this system, the press-focused single element lithium niobate ($LiNbO_3$) transducer [Fig. 2(a)] was constructed via the conventional procedure [23] to both generate acoustic radiation force, which push a target sample, and detect photoacoustic signals from the sample. The center frequency of the transducer was 30 MHz [Fig. 2(b)]. The aperture diameter of the transducer was 4 mm with a focal length of 3 mm (*f*-number = 0.75). The lateral beam profile [Fig. 2(c)] was measured with a calibrated hydrophone which yielded the pressure level at a given input voltage to the transducer. The beam width was measured to be 37 µm. In addition, the peak acoustic pressures at focus were measured. The peak acoustic pressures were 0.76, 1.00, 1.39, 2.16, 2.93, and 3.71 MPa when the input voltages were 2, 5, 10, 20, 30, and 40 V_{pp}, respectively [Fig. 2(d)].

The alignment of the focus of a transducer at the center of a laser beam is of critical importance in achieving the maximum sensitivity in the detection of PA signals from a target. To do so, we first aligned the focus of the transducer at the center of the image field of view with a 6 µm tungsten wire with a procedure described previously [Fig. 2(e), upper] [19]. After that, the laser beam center was aligned at the center of the image field of view using fluorescence imaging of 10 µM Rhodamine B diluted with HBBS (Em: ~580 nm) [Fig. 2(e), lower]. Figure 2(e) (upper) illustrates the tungsten wire alignment in the horizontal and vertical direction at the center of the image field of view.

3.2 Measurement of mechanical properties of phantoms with different Young's modulus

For the evaluation of the PA-ARFI microscopic system developed, we first investigated its capability in the detection of axial displacement of a target sample in the phantom. For a 0.5 µm initial movement of the target sample, the target position was measured to be 0.3 µm with the PA-ARFI microscopy. In contrast, at 1 and 1.5 µm movements, the target positions were

#221587 - $15.00 USD Received 26 Aug 2014; revised 25 Sep 2014; accepted 2 Oct 2014; published 3 Dec 2014
(C) 2014 OSA

measured to be 0.7 and 1.25 µm from the initial position, respectively [Fig. 3(a)]. The discrepancy between the measured and real target position was 0.25 µm at 1.5 µm target movement. This result suggested that the PA-ARFI microscopy had the capability to detect at least a 0.5 µm displacement of a target sample. Although the discrepancy might be the error of the positioner caused by the backlash of the step-motor [24], which was here utilized to position the target sample to a certain location, it is smaller than the expected measurement resolution of 0.75 µm calculated by the sampling rate.

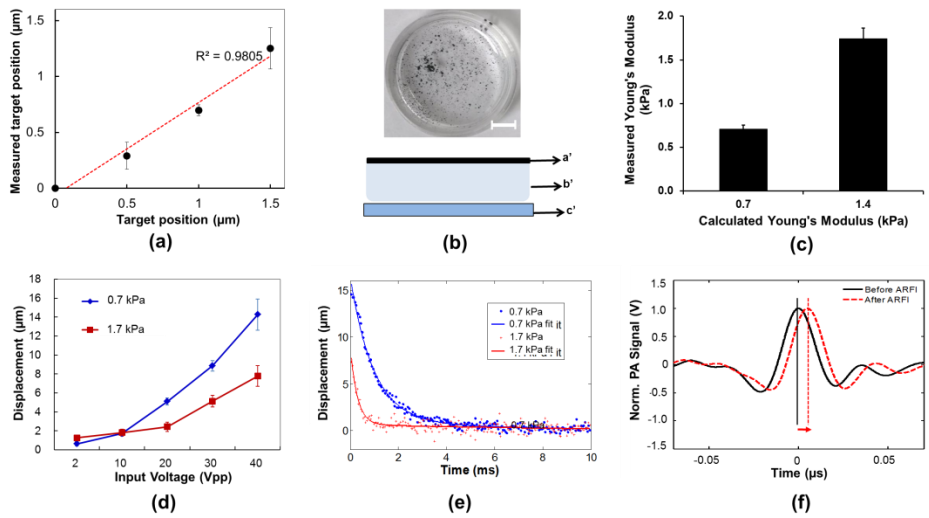

Fig. 3. Evaluation of PA-ARFI microscopy with agar phantoms. (a) Target position measured using PA-ARFI microscopy versus real target position. (b) Geometry of a tissue mimicking agar phantom. Photograph of the phantom (upper) and phantom layers (lower) consisting of a FCNT (a'), agar gel (b'), and substrate layer (c'). The scale bar indicates 5 mm. (c) Comparison of between measured Young's Moduli and calculated Young's moduli of phantoms. (d) Displacements of FCNTs in phantoms with the indicated Young's moduli, 0.7 and 1.7 kPa, due to acoustic radiation forces at the given voltage inputs to the transducer (2, 10, 20, 30, and 40 V_{pp}). (e) Temporal displacement changes of target FCNTs in the indicated phantoms at the driving voltage = 40V_{pp} (representative ones). (f) Temporal displacement of PA signals before and after ARFI application on 1.7 kPa phantom (driving voltage: 40 V_{pp}). An arrow indicates the displacement direction.

In addition, we further examined the elasticity of agar phantoms using the PA-ARFI microscopic system. Before carrying out this phantom study, we measured the elasticity of the constructed agar phantoms using an Electro Force Load Frame System [Fig. 3(b)]. The Young's moduli were measured to be ~0.7 and ~1.7 kPa for the phantoms with the calculated Young's moduli of 0.7 and 1.4 kPa, respectively [Fig. 3(c)]. These results here showed that the measured Young's modulus of the phantom was slightly higher than the calculated Young's modulus at 1.4 kPa. The discrepancy at 1.4 kPa may be caused by water evaporation during fabrication of the phantoms.

After the elasticity of the phantoms was measured, we investigated whether the PA-ARFI microscopy allowed discrimination between the agar phantoms with the indicated elasticity. When the input voltages were 2 and 10 V_{pp}, which generated the acoustic pressures of 0.76 and 1.39 MPa at focus, the displacements of FCNTs in all the phantoms were less than 2 µm [Fig. 3(d)]. In contrast, when the input voltage was increased to 20 V_{pp}, the displacements of FCNTs in the phantoms with the measured Young's modulus of 0.7 and 1.7 kPa were increased by ~5.1 µm and ~2.43 µm, respectively. Moreover, the displacements of FNCTs in each phantom were increased by 14.78 µm (measured Young' modulus: 0.7 kPa) and 7.78 µm (measured Young' modulus: 1.7 kPa), respectively as the input voltage was further increased

#221587 - $15.00 USD Received 26 Aug 2014; revised 25 Sep 2014; accepted 2 Oct 2014; published 3 Dec 2014
(C) 2014 OSA

by 40 V_{pp} (corresponding acoustic pressure: 3.7 MPa). The mean displacement of FCNTs in the phantom with measured Young's modulus of 0.7 kPa was here almost two-fold higher than that in the phantom with the measured Young's modulus of 1.7 kPa [Fig. 3(d)]. Figure 3(e) describes the temporal displacement changes of FCNTs in each phantom due to acoustic radiation force at 40V_{pp}. The peak displacement in the soft phantom (0.7 kPa) was almost two times higher than that in the harder phantom (1.7 kPa). The target FCNTs in the harder phantom (1.7 kPa) returned to the original position in less than 2 ms, whereas it took longer than 5 ms in the soft phantom (0.7 kPa). Figure 3(f) illustrates the temporal displacement of PA-signals from FCNTS before and after ARFI application to the phantom with Young's modulus at 1.7 kPa. The PA signals were detected at the later time after ARFI application than before ARFI application, indicating the FCNTs displacement due to the ARFI application [Fig. 3(f)]. In these results, it is important to note that the Young's modulus of FCNTs (over 1 kPa) utilized is much higher than the Young's moduli of the phantoms [25], suggesting that the displacements of FCNTs approximated well the displacements of agar phantoms surrounding target FCNTs. Taken together, these results demonstrated that PA-ARFI microscopy was capable of probing the mechanical properties of specimens with different Young's modulus, suggesting that it may be suited for use in the estimation of mechanical properties of cells with different Young's modulus *in vitro*.

3.3 Measurement of mechanical properties of different types of breast cancer cells

The phantom study showed that the PA-ARFI microscopy was capable of probing mechanical properties of the phantoms with different Young's modulus and thereby differentiating between them. As the next step, we employed the PA-ARFI microscopy to measure mechanical properties of cancer cells including MDA-MB-231 (highly-metastatic), SKBR3 (weakly-metastatic), and MCF-7 (weakly-metastatic). In particular, we compared the displacements of FCNTs binding to cancer cell membrane at the given voltage of 40 V_{pp}, which was the highest voltage utilized in the phantom study enabling the measurement of mechanical properties of a sample with Young's modulus of approximately 1.7 kPa. By employing the experimental procedures described in Fig. 4(a), the membrane displacements of each cell type due to acoustic radiation force acting on the cells were measured. The mean membrane displacement of MDA-MB-231 human breast cancer cells (2.64 ± 1.50 μm) due to the applied acoustic radiation force impulses was significantly greater than that of SKBR3 (1.50 ± 0.94 μm) (p-value = 0.0089 < 0.01) and MCF-7 human breast cancer cells (1.10 ± 0.47 μm) (p-value = 0.0059 < 0.01). In contrast, the mean membrane displacement of SKBR3 human breast cancer cells was not significantly different from that of MCF-7 human breast cancer cells (p-value = 0.2989 > 0.01). The standard deviation may be generated by both the variation in the cell stiffness and the inherent measurement error of 0.75 μm caused by the sampling rate. In this experiment, we tested a total of 30 individual cells for each type of cancer cells. ARFI application induced membrane displacement in all MDA-MB-231 cells among the 30 cells. In contrast, in only twenty-one SKBR3 and ten MCF-7 cells among a total of thirty, cells membrane displacement was observed upon ARFI application. It may be attributed to the fact that SKBR3 and MCF-7 cells are stiffer than MDA-MB-231 cells, suggesting that the stronger ARFI may be needed to deform SKBR3 and MCF-7 cells. This may be achieved by increasing the input voltage to the transducer. However, in this study, the input voltage to the transducer was limited to 40 V_{pp} since the higher voltage of the bursts with such duty cycle may damage the transducer. Figure 4(c) demonstrates the distributions of membrane displacement. In the histogram of membrane displacements of each type of cells, MDA-MB-231 cells showed a peak at 2μm in the displacement, whereas SKBR3 and MCF-7 cells a peak at 1μm. Meanwhile, the MDA-MB-231 cells exhibited a wider distribution as well as more frequencies in the displacement greater than 2 μm than both SKBR3 and MCF-7 cells. In particular, several MDA-MB-231 cells exhibited cell membrane displacement of greater than 5 μm upon ARFI application [Fig. 4(c)], indicating that the

#221587 - $15.00 USD Received 26 Aug 2014; revised 25 Sep 2014; accepted 2 Oct 2014; published 3 Dec 2014
(C) 2014 OSA

SKBR3 and MCF-7 cells might be stiffer than MDA-MB-231 cells corroborating previous AFM studies, which showed that the highly-invasive MDA-MB-231 breast cancer cells were mechanically softer than both non-transformed breast epithelium cells and weakly invasive breast cancer MCF-7 cells [26]. In addition, the relaxation time for MDA-MB-231 cells was much longer than those for MCF-7 and SKBR-3 cells [Fig. 4(d)], may indicate the additional evidence that MDA-MB-231 cells are softer than MCF-7 and SKBR-3 cells.Young's modulus of the MDA-MB-231 cells in the previous literature was found to be ~500 Pa and ~750 Pa in nuclear and cytoplasmic regions, respectively. In contrast, Young's modulus of MCF-7 cells was found to be ~800 Pa and ~1300 Pa in those regions, respectively. In our study, MDA-MB-231 cells were found to exhibit a larger membrane displacement than MCF-7 cells upon the ARFI application at 3.7 MPa, indicating that MDA-MB-231 cells were softer than MCF-7 cells. It is therefore reasonable to conclude that our PA-ARFI method is capable of discriminating between cells with different mechanics at the single cell level *in vitro*.

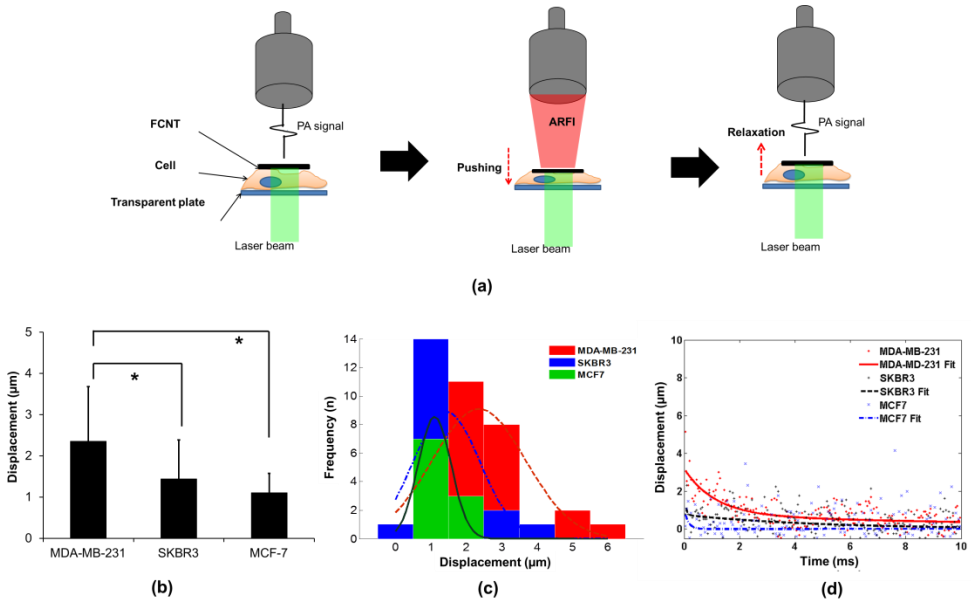

Fig. 4. Membrane displacement of different types of cancer cells due to applied acoustic radiation force (input voltage: 40 Vpp). (a) Diagram of PA-ARFI microscopy of cells. After positioning of a target cell labeled with FCNTs at the center of the image field of view (left), acoustic radiation force impulses were applied onto the cells (middle) and followed by tracking of cell membrane displacements (right). (b) Mean cell membrane displacement of MDA-MB-231 (n = 30), SKBR3 (n = 21), and MCF-7 (n = 10) cells (*: p-value < 0.01). (c) Histogram of membrane displacements of each cell type (red: MDA-MB-231, blue: SKBR3, green: MCF-7). The dotted graphs represent Gaussian distributions. (d) Temporal displacement changes of FNTs attached to the membrane of target cells (representative ones).

A wide range of tools, including atomic force microscopy (AFM), cell stretching, and microrheology, have been used to assess cellular mechanics in both the cytoplasm and nucleus of metastatic or non-metastatic cancer cells [26–29]. The results reported in this paper indicated that this non-contact approach was a viable alternative. They also showed that the PA-ARFI microscopic system with a transducer at 30 MHz had limitations in assessing more localized regions of the cells (the data are not shown) since the pushing area limited by the lateral beam size of 37 μm is broad enough to cover the whole single cell surface. However, this shortcoming may be overcome by increasing both the center frequency of a transducer and improving the lateral beam width of the laser light for photoacoustic generation.

#221587 - $15.00 USD Received 26 Aug 2014; revised 25 Sep 2014; accepted 2 Oct 2014; published 3 Dec 2014
(C) 2014 OSA

Instead of using the photoacoustic detection method, other ultra-high speed imaging techniques [30] may be applied to monitor membrane displacement of cells due to acoustic radiation force impulse applications in the estimation of mechanical properties of the cells. However, in order to track the displacement of the membrane of an object with a Young's modulus greater than 1.7 kPa, which would return to its original position in less than 2 ms following initial disturbance, the image acquisition rate needs to be greater than 1 kHz according to Nyquist criteria. Furthermore, sophisticated imaging components are required, thereby increasing the cost. In contrast, the PA-ARFI method reported here allowed the tracking of membrane displacement with a relatively simple experimental arrangement consisting of a single transducer and thus enable to estimate the elasticity of cells with Young's modulus of higher 1.7 kPa which can be achieved by increasing the pushing beam energy e.g. increasing the PRF or the number of cycles.

To date, carbon nanotubes (CNTs) have been utilized for various cell applications. The biocompatibility of CNTs has been shown to differ in different types of cells [31]. Single-walled (SW) CNTs have been shown to block potassium channel activities in heterologous mammalian cell systems, suggesting a degree of cytotoxicity [32]. In contrast, the SWCNTs under the culture medium do not significantly affect the macrophages and leukemia cells [33, 34]. Moreover, the functionalized SWCNTs are non-toxic to primary immune cells. Therefore, they have been widely utilized as a contrast agent in medical imaging as well as a carrier molecule for the delivery of therapeutically active molecules to target cells [35]. In this study, the results had a good agreement with the results obtained in previous studies, of which MDA-MB-231 cells exhibited softer than MCF-7 and SKBR-3 cells, suggesting that FCNTs may not significantly alter the mechanical properties of breast cancer cells and therefore they can be utilized as a contrast agent in the measurement of mechanics of breast cancer cells using the PA-ARFI microscopic method. However, to apply this PA-ARFI microscopic method to other types of cells, it would be necessary to test the FCNT cytotoxicity since the FCNT cytotoxicity has shown to be heterogeneous in the different types of cells [31, 36].

High-intensity laser light with long exposure time may induce cell damages due to reactive oxygen species generation. Therefore, it is necessary to apply low intensity light to cells to avoid phototoxicity during live cell imaging [37]. In this study, we applied the pulsed laser light to breast cancer cells for very short duration (25 ms) in order to avoid phototoxicity during photoacoustic signal excitation. We did not hence observe any notable cell morphological changes such as cell blebbing and shrinkage after application of laser light to the cells for photoacoustic signal excitation. In the previous study, the 532nm pulsed laser light at less 36 mJ cm^{-2} did not induce any significant changes in viability of cancer cells [38]. Note that the total fluence of the applied laser light for photoacoustic signal excitation (< ~9mJ cm^{-2}) was here much less than the light dose used in the previous study. However, for more accurate examination of phototoxicity effects on the cell, it would be necessary to test cell viability after the light application using cell viability assay.

4. Conclusion

This paper reports a novel non-contact PA-ARFI microscopic method capable of probing mechanical properties of a single cell. PA-ARFI microscopy allowed measurement of the mechanical properties of targets of varying Young's modulus. Here FCNTs enabled the tracking of targeted sample displacement induced by acoustic radiation forces acting on the sample with high sensitivity. In particular, this method makes it possible to measure the mechanical properties of breast cancer cells, thus enabling to discriminate them relatively. To test its feasibility, experiments were performed on cancer cells of different phenotype. The results show that invasive MDA-MB-231 cells were less stiff than less invasive SKBR3 and MCF-7 cells corroborating previous studies that MDA-MB-231 cells are less stiff than SKBR3 and MCF-7 cells [26]. To apply this method to other types of cells, the FCNT may be

#221587 - $15.00 USD Received 26 Aug 2014; revised 25 Sep 2014; accepted 2 Oct 2014; published 3 Dec 2014
(C) 2014 OSA

replaced with other contrast agents, which do not significant affect their mechanical properties. As a result, it appears that this non-contact PA-ARFI method may offer a viable alternative in the measurement of mechanical properties of a single cell. Finally, it is important note that the developed PA-ARFI microscopic system is the first ultrasonic palpation system for measurement of mechanical properties of a single cell.

Acknowledgments

This work has been supported by the NIH grants (R01-EB012058, and P41-EB2182) to K.K. Shung and the DGIST R&D Program of the Ministry of Science, ICT and Technology of Korea (14-IT-01 and 2014060005) to J.Y. Hwang.